Electronic Supplementary Material (ESI) for Nanoscale.

Supporting information

Fast-switching electrochromic properties of mesoporous WO_3 films with oxygen vacancy defects

Bon-Ryul Koo[a] and Hyo-Jin Ahn[*ab]

[a]Program of Materials Science & Engineering, Convergence Institute of Biomedical Engineering and Biomaterials, Seoul National University of Science and Technology, Seoul 01811, Korea

[b]Department of Materials Science and Engineering, Seoul National University of Science and Technology, Seoul 01811, Korea

EXPERIMENTAL SECTION

Fabrication of mesoporous WO_3 films with oxygen vacancy defects

Mesoporous WO_3 films with oxygen vacancy defects were fabricated on commercial FTO glass (Pilkington, 8.0 Ω/□) using the camphene-assisted sol-gel method. The precursor solution for deposition of mesoporous WO_3 films with oxygen vacancy defects was prepared by dissolving tungsten (Ⅵ) chloride (WCl_6, Aldrich) in 2-propanol ($(CH_3)_2CHOH$, Aldrich). Camphene ((Hill Notation)$C_{10}H_{16}$, Aldrich) used as an organic additive was then added into the above-prepared solutions with stirring at room temperature. The relative weight ratios of the added camphene to the solvent were controlled to be 0, 5, 10, and 15 wt% for optimizing the EC properties of the mesoporous WO_3 films with oxygen vacancy defects. The resultant solutions were spin-coated on the FTO glasses and then annealed at 300 °C in air to form the mesoporous WO_3 films with oxygen vacancy defects. Therefore, four types of samples were fabricated by the camphene-assisted sol-gel method with the different weight ratios of the added camphene (0, 5, 10, and 15 wt%; thereafter denoted as bare WO_3, WO_3/C5, WO_3/C10, and WO_3/C15, respectively).

Characterization

The thermal behaviour of the samples was investigated by the thermogravimetric analysis (TGA, TGA−50, Shimadzu). The morphological properties was observed by a field-emission scanning electron microscopy (FESEM, Hitachi S−4800). The chemical state and crystal structure were investigated through X-ray photoelectron spectroscopy (XPS, ESCALAB 250 equipped with an Al K_α X-ray source) and X-ray diffraction (XRD, Rigaku D/Max−2500 diffractometer using Cu K_α radiation), respectively. The electrical properties were confirmed by a Hall-effect measurement system (Ecopia, HMS-3000). The electrochemical and electrochromic properties were measured using a

potentiostat/galvanostat (PGSTAT302N, FRA32M, Metrohm Autolab B.V., Netherlands) in a three-electrode electrochemical cell with 1 M $LiClO_4$ electrolyte, in which Pt wire and Ag wire were used as the counter and reference electrodes, respectively. The measurement of *in situ* optical properties was performed using ultraviolet-visible (UV−vis) spectroscopy (Perkim−Elmer, Lambda−35) in the wavelength range between 400 and 800 nm. The electrochemical impedances test was carried out on this electrochemical cell at the frequency range of 100 kHz to 0.1 Hz. The cycling stability was characterized by tracing the transmittance modulation at 633 nm during 1,000 cycles in the potential region of −0.7−1.0 V.

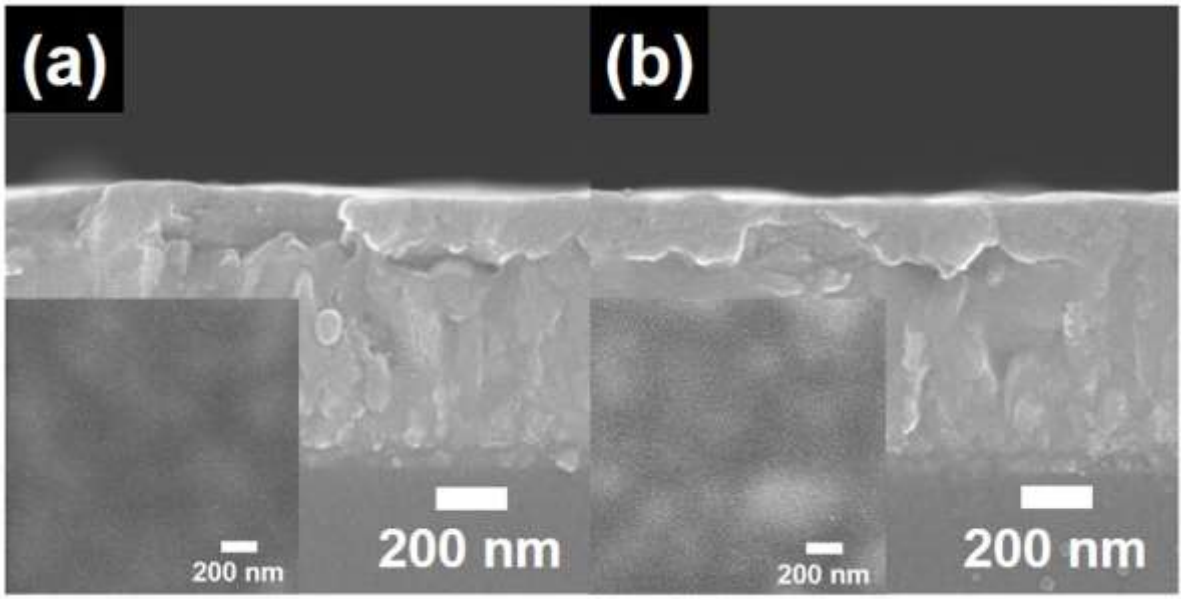

Fig. S1 Cross-view SEM images of (a) bareWO_3 and (b) WO_3/C10 before the annealing. The insets in show top-view SEM images.

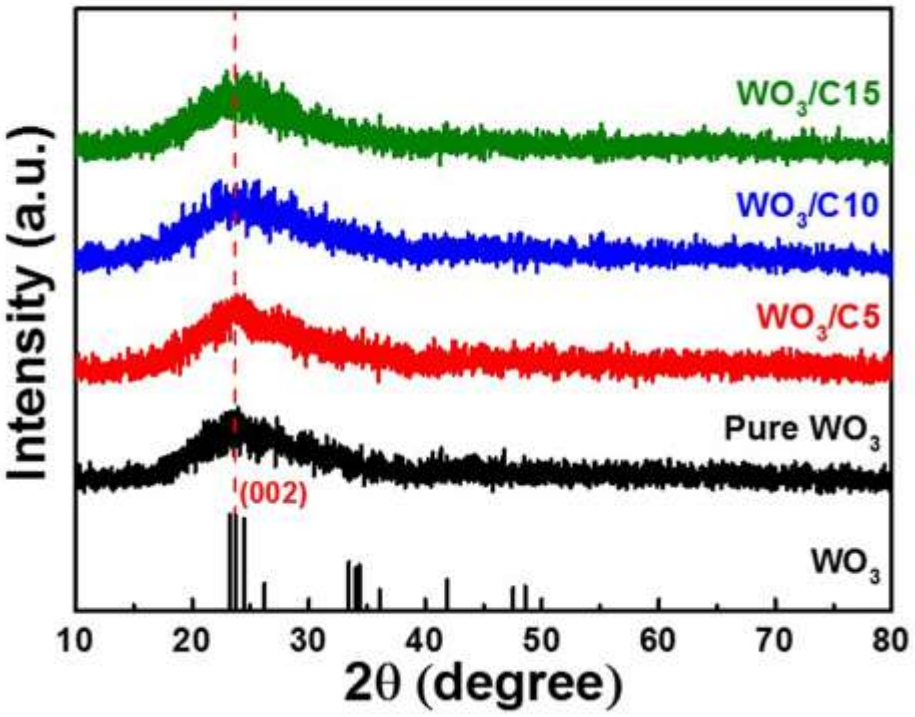

Fig. S2 XRD curves of bare WO_3, WO_3/C5, WO_3/C10, and WO_3/C15.

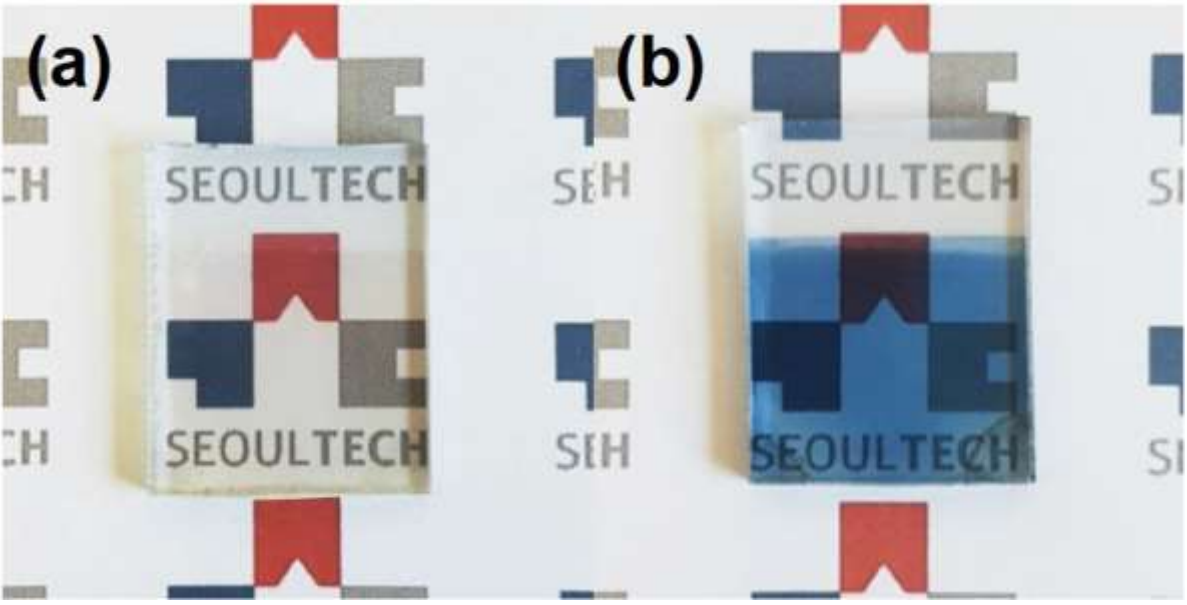

Fig. S3 Photographs of mesoporous WO_3 films with oxygen vacancy defects (WO_3/C10) with 2.5 × 2.0 cm in size in (a) the bleached and (b) coloured states.

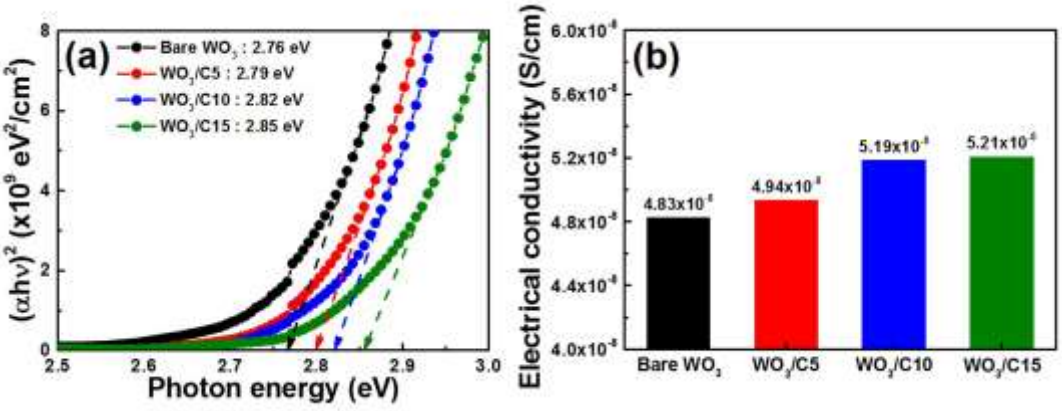

Fig. S4 (a) Plots of $(ahv)^2$ versus photon energy and (b) electrical conductivity obtained from bare WO_3, WO_3/C5, WO_3/C10, and WO_3/C15.

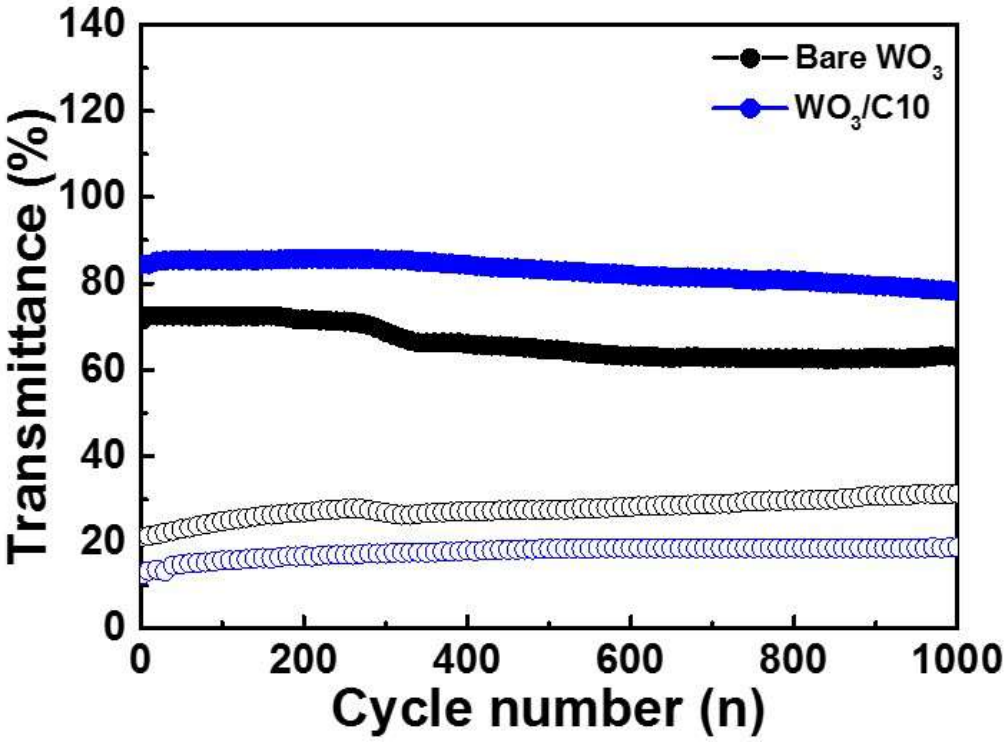

Fig. S5 Cycling stability of transmittance modulation at 633 nm obtained from bare WO_3 and WO_3/C10, applied at 1.0 V for bleached state (solid line) and −0.7 V for coloured state (dotted line).

Table S1 Comparison of EC properties from previously reported WO_3-based materials.

Material	Transmittance modulation (%, 633 nm)	Coloration speed (s)	Bleaching speed (s)	CE (cm^2/C)
Nest-like $WO_3 \cdot 0.33H_2O$ films[1]	-	26.0	5.5	126.3
Cylinder-like WO_3 nanorod arrays[9]	64.0	6.0	5.0	61.0
Macroporous WO_3 films[10]	-	5.1	8.7	50.1
Porous WO_3 films[15]	-	-	-	38.0
WO_3 nanoparticle films[34]	-	-	-	42.0
Mesoporous WO_3 films[28]	76.7	6.4	6.0	50.6
Mesoporous WO_3 films[39]	75.0	10.0	10.0	50.0
Disordered porous semicrystalline WO_3 films[40]	-	4.2	5.5	32.3
Vertically aligned hierarchical WO_3 arrays[41]	66.0	4.6	3.6	120.0
WO_3 micro-unchin films[42]	-	-	-	42.3
Homogenous WO_3 films[43]	-	-	-	28.0
Highly crystalline WO_3 films[44]	-	3.0	9.0	40.0
WO_3 crystalline nanoparticle films[45]	-	9.0	15.0	51.0
Mesoporous WO_3 films with oxygen vacancy defects	74.6	5.8	1.0	51.4